

# Unified theory of atom-centered representations and graph convolutional machine-learning schemes

Jigyasa Nigam,<sup>1,2</sup> Guillaume Fraux,<sup>1</sup> and Michele Ceriotti<sup>1,2,\*</sup>

<sup>1</sup>*Laboratory of Computational Science and Modeling, Institute of Materials, École Polytechnique Fédérale de Lausanne, 1015 Lausanne, Switzerland*

<sup>2</sup>*National Centre for Computational Design and Discovery of Novel Materials (MARVEL), École Polytechnique Fédérale de Lausanne, 1015 Lausanne, Switzerland*

Data-driven schemes that associate molecular and crystal structures with their microscopic properties share the need for a concise, effective description of the arrangement of their atomic constituents. Many types of models rely on descriptions of atom-centered environments, that are associated with an atomic property or with an atomic contribution to an extensive macroscopic quantity. Frameworks in this class can be understood in terms of atom-centered density correlations (ACDC), that are used as a basis for a body-ordered, symmetry-adapted expansion of the targets. Several other schemes, that gather information on the relationship between neighboring atoms using graph-convolutional (or message-passing) ideas, cannot be directly mapped to correlations centered around a single atom. We generalize the ACDC framework to include multi-centered information, generating representations that provide a complete linear basis to regress symmetric functions of atomic coordinates, and form the basis to systematize our understanding of both atom-centered and graph-convolutional machine-learning schemes.

The understanding that  $\nu$ -point correlations of the atom density provide a complete linear basis to expand any property of these atom-centered environments<sup>1–3</sup> sheds light on the relations between different machine-learning (ML) frameworks for atomistic modeling,<sup>4–6</sup> and is driving much progress in obtaining more accurate and performant schemes<sup>7</sup>. This systematic approach is somewhat disconnected from efforts that combine ideas from geometric ML<sup>8</sup> and point clouds<sup>9,10</sup>, that look at molecules as graphs in which the atoms play the role of nodes, and the interatomic distances decorate the edges that connect them<sup>11–16</sup> – a point of view that has a long-standing tradition in the field of cheminformatics<sup>17,18</sup>. With the rise of equivariant neural networks<sup>9,19–24</sup> the similarity between atom-centered and message-passing (MP) schemes has become more and more apparent, since both rely on symmetry-adapted constructions

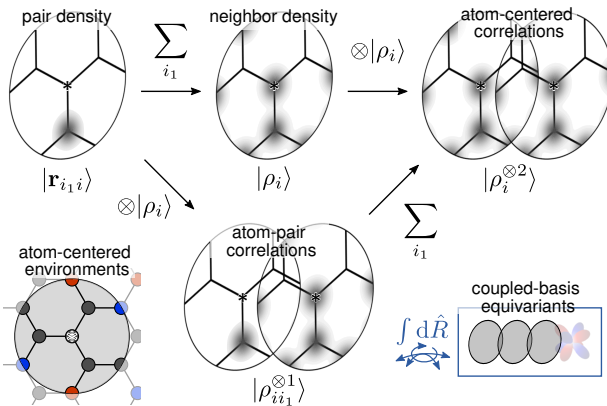


Figure 1: A few examples of ACDC representations, and their construction by summing pair contributions over atomic neighbors.

based on  $O(3)$ -preserving operations. We introduce a formalism to define representations which incorporate MP ideas, provide a linear basis to expand symmetric functions of the relative position of atoms (or points in a 3D cloud) and are similar in spirit to a wide variety of equivariant graph convolutional schemes. We give examples of the performance of these graph-convolutional representations in describing short- and long-range structure-property relations, and discuss the potential of this framework to unify different approaches to geometric machine learning.

## I. THEORY

*a. Atom-centered density correlations.* The basic ingredient in the atom-centered density correlation (ACDC) framework<sup>2</sup> involves localized functions (e.g. Gaussians  $g$  or Dirac  $\delta$  distributions) centered at the atomic positions  $\mathbf{r}_i$ . Following the notation formalized in Section 3.1 of Ref. 4, we indicate these atomic contributions as  $\langle \mathbf{x} | \mathbf{r}_i \rangle \equiv g(\mathbf{x} - \mathbf{r}_i)$  (or  $\delta(\mathbf{x} - \mathbf{r}_i)$ ). Repeated symmetrization, and summation over the neighbors of the central atom, yield a family of  $(N + 1)$ -centers,  $(\nu + 1)$ -body-order equivariant representations,<sup>25</sup>

$$|\rho_{ii_1 \dots i_N}^{\otimes \nu} ; \sigma ; \lambda \mu \rangle \equiv \int_{O(3)} d\hat{R} \hat{R} |\lambda \mu \rangle \otimes \hat{R} |\sigma \rangle \otimes \hat{R} |\rho_{ii_1 \dots i_N}^{\otimes \nu} \rangle. \quad (1)$$

In this expression,  $|\lambda \mu \rangle$  and  $|\sigma \rangle$  are vectors that track the spherical irrep and the parity label of the representation.  $|\rho_{ii_1 \dots i_N}^{\otimes \nu} \rangle$  indicates a tensor product of pair terms  $|\mathbf{r}_{i_k i} \rangle$ , that determine the relative position  $\mathbf{r}_{i_k i} = \mathbf{r}_{i_k} - \mathbf{r}_i$  of the  $N$  centers around the central atom, and of  $\nu$  of the neighbors found within the  $i$ -centered environment  $A_i$

$$|\rho_{ii_1 \dots i_N}^{\otimes \nu} \rangle = |\mathbf{r}_{i_1 i} \rangle \otimes \dots \otimes |\mathbf{r}_{i_N i} \rangle \otimes \sum_{j_1 \dots j_\nu \in A_i} |\mathbf{r}_{j_1 i} \rangle \otimes \dots \otimes |\mathbf{r}_{j_\nu i} \rangle. \quad (2)$$

Eq. (2) is a highly abstract formulation of the construction (represented schematically in Fig. 1), that

\* michele.ceriotti@epfl.ch

can be evaluated in practice by projection on any complete basis  $|q\rangle$ . By combining the resulting coefficients with appropriately fitted weights  $\langle y|q\rangle$ , one can approximate any  $(N+1)$ -center quantity  $y_{ii_1\dots i_N}$  that is symmetric with respect to permutations of the labels of the neighbors, and that is equivariant with respect to rigid translations and rotations, e.g.

$$y_{ii_1\dots i_N}^{\sigma, \lambda\mu}(A) = \sum_q \langle y; \sigma; \lambda|q\rangle \langle q|\rho_{ii_1\dots i_N}^{\otimes\nu}; \sigma; \lambda\mu\rangle. \quad (3)$$

To see how, one can consider a real-space basis and a  $\delta$ -like atom density. For an invariant (scalar) property,

$$y_{ii_1\dots i_N}(A) = \int d\{\mathbf{x}\} \langle y|\{\mathbf{x}\}\rangle \langle \{\mathbf{x}\}|\delta_{ii_1\dots i_N}^{\otimes\nu} = \int_{O(3)} d\hat{R} \sum_{j_1\dots j_N \in A_i} \tilde{y}(\hat{R}\mathbf{r}_{j_1i}, \dots, \hat{R}\mathbf{r}_{j_Ni}, \hat{R}\mathbf{r}_{i_1i}, \dots, \hat{R}\mathbf{r}_{i_Ni}), \quad (4)$$

where  $\{\mathbf{x}\}$  is a shorthand for the collection of the continuous indices associated with each interatomic degree of freedom.<sup>26</sup>

Explicitly evaluating the sum over neighbors entails a cost that scales exponentially with  $\nu$ . However, a *density trick* eliminates the steep scaling with the number of neighbors, by first computing an atom-centered density,  $|\rho_i\rangle \equiv \sum_j |\mathbf{r}_{ji}\rangle$ , and then performing the tensor products.<sup>4</sup> Similarly, one does not need to compute the integral over rotations explicitly. By expressing the equivariant features in an irreducible *coupled* basis, and discretizing each term in the tensor product on a basis of radial functions  $\langle x|nl\rangle$  and spherical harmonics  $\langle \hat{\mathbf{x}}|lm\rangle$ , the full set of symmetry-adapted equivariants (1) can be evaluated by combining symmetry-adapted terms in an iterative fashion<sup>27</sup>

$$\begin{aligned} & \langle q_1l_1; q_2l_2|A_1; A_2; (\sigma_1\sigma_2(-1)^{l_1+l_2+\lambda}); \lambda\mu\rangle = \\ & \sum_{m_1m_2} \langle q_1|A_1; \sigma_1; l_1m_1\rangle \langle q_2|A_2; \sigma_2; l_2m_2\rangle \langle l_1m_1; l_2m_2|\lambda\mu\rangle. \end{aligned} \quad (5)$$

Thus, expressions such as (2) provide a notation to indicate a linear basis to approximate properties of  $(N+1)$  atomic centers that depend simultaneously on the positions of  $\nu$  neighbors, and (5) a strategy to compute such features iteratively, while keeping the irreducible equivariant components separate.

*b. Graph-convolutional representations.* The ACDC construction is entirely based on terms centered around a single atom, and can be seen as alternative to graph-convolutional (GC) architectures, which are based on the idea that information on multiple nodes (atoms, in this context) and their connectivity (inter-atomic distance vectors) could be combined to provide higher descriptive power. The essential ideas behind GC frameworks are summarized in Fig. 2. We refer the reader to Refs. 11,28 for an overview of the methodology.

The ACDC framework can be extended to provide a basis for the construction of arbitrarily complex equivariant GC frameworks. First, we introduce the possibility of decorating an  $(N+1)$ -center representation

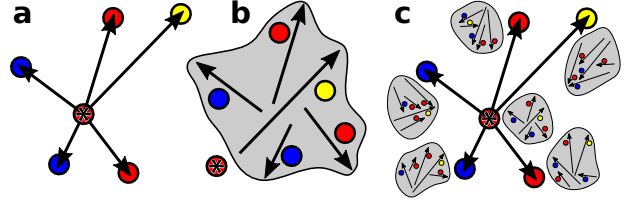


Figure 2: Schematic representation of the functioning of graph convolutional schemes. (a) A description of the connectivity of a selected node  $i$  with each of its neighbors  $j$  is built by combining information on the neighbor attributes, and on the geometry of the connection; (b) Information on all the neighbors of the selected node is combined in a way that is independent on the order by which they are considered; (c) The compound description of the neighborhood is assigned as the new attributes of the central node. Iterating the process propagates to every node information on the neighbors' neighbors.

with information on *any* of the centers. Disregarding the symmetry indices and the integral over rotations for simplicity — as discussed above, symmetry-adapted equivariants can be obtained by using Eq. (5) on the tensor-product pattern — we define the decorated atom-density representations

$$|\rho_{ii_1\dots i_N}^{\otimes\nu\nu_1\dots\nu_N}\rangle \equiv |\rho_i^{\otimes\nu}\rangle \otimes |\rho_{i_1}^{\otimes\nu_1}\rangle \otimes |\mathbf{r}_{i_1i}\rangle \dots \otimes |\rho_{i_N}^{\otimes\nu_N}\rangle \otimes |\mathbf{r}_{i_Ni}\rangle. \quad (6)$$

The  $(N+1)$ -center representations (2) are a special case, with  $\nu_{k>0} = 0$ . Given that we encode information on the *vectors* connecting the central atom  $i$  with its neighbors  $\mathbf{r}_{i_ki}$ , the information on the position of the neighbors relative to each other is also formally retained, because  $\mathbf{r}_{i_ki_k} = \mathbf{r}_{i_ki} - \mathbf{r}_{i_ki}$ .

Simple GC-like representations can be obtained starting from decorated pair features, and summing over the pair index (Fig. 3):

$$|\rho_i^{\otimes[\nu\leftarrow\nu_1]}\rangle \equiv \sum_{i_1} |\rho_{ii_1}^{\otimes\nu\nu_1}\rangle = |\rho_i^{\otimes\nu}\rangle \otimes \sum_{i_1} |\rho_{i_1}^{\otimes\nu_1}\rangle \otimes |\mathbf{r}_{i_1i}\rangle. \quad (7)$$

For the case of  $\nu_1 = 0$ , the sum simplifies to  $|\rho_i\rangle$ , thus the expression simply evaluates ACDC features of order  $\nu + 1$ . By expanding the tensor product, and in analogy with (4), one sees that these features provide a linear basis to expand a symmetrized function of the neighbors of  $i$  and of each of their neighbors, e.g.

$$\sum_q \langle y|q\rangle \langle q|\rho_i^{\otimes[1\leftarrow 1]}\rangle = \sum_{i_1, j \in A_i; j_1 \in A_{i_1}} \tilde{y}(\mathbf{r}_{ji}, \mathbf{r}_{i_1i}, \mathbf{r}_{j_1i_1}). \quad (8)$$

A basis for  $O(3)$ -equivariant predictions can be obtained by computing the tensor product iteratively in the coupled basis, following (5). Except for the (important) subtlety that one of the indices extends over the neighborhood of  $i_1$ , these features contain the same information as the  $\nu = 3$  ACDC (the bispectrum). One can verify that  $|\rho_i^{\otimes[1\leftarrow 1]}\rangle$  discriminates between structures that are degenerate<sup>29</sup> for the

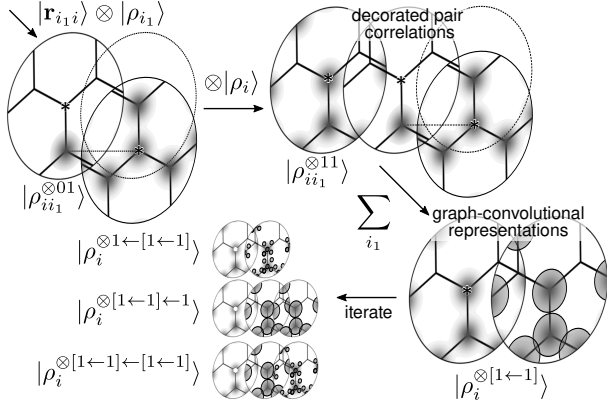


Figure 3: Construction of GC features from the contraction of pair and neighbor-density terms. The process can be iterated in many different ways (see the SM for details).

on-site powerspectrum  $|\rho_i^{\otimes 2}\rangle$ , but cannot discriminate between environments that have the same  $|\rho_i^{\otimes 3}\rangle$ .

Eq. 7 can be generalized in different ways. For example, one could compute  $N = 2$  decorated features and contract them

$$|\rho_{ii_1}^{\otimes[\nu \leftarrow \nu_2]\nu_1}\rangle \equiv \sum_{i_2} |\rho_{ii_1 i_2}^{\otimes\nu\nu_1\nu_2}\rangle. \quad (9)$$

These features describe atomic pairs as a sum over descriptors of triplets. They could be used as features to characterize edges, and seen as a building block of GC architectures that use bonds as nodes and angles as edges<sup>30</sup>.

By also summing over  $i_1$ , one obtains graph-convolutional ACDC features that contain joint information on two decorated neighbors:

$$|\rho_i^{\otimes[\nu \leftarrow (\nu_1, \nu_2)]}\rangle = \sum_{i_1 i_2} |\rho_i^{\otimes\nu}\rangle \otimes |\mathbf{r}_{i_1 i}\rangle \otimes |\rho_{i_1}^{\otimes\nu_1}\rangle \otimes |\mathbf{r}_{i_2 i}\rangle \otimes |\rho_{i_2}^{\otimes\nu_2}\rangle. \quad (10)$$

This corresponds to an overall correlation order of  $\nu + \nu_1 + \nu_2 + 2$  neighbors around the the  $i$ -atom. More generally, representations that incorporate joint information on multiple neighbors can be built starting from pair GC features — see the supplementary material (SM) for more information:

$$|\rho_i^{\otimes[\nu \leftarrow \nu_1]}\rangle \otimes |\rho_i^{\otimes[\nu' \leftarrow \nu'_1]}\rangle = |\rho_i^{\otimes[(\nu + \nu') \leftarrow (\nu_1, \nu'_1)]}\rangle. \quad (11)$$

Note that the left-hand side avoids the double sum over neighbors in Eq. (10), similar to how the density trick avoids summation over tuples of neighbors by first expanding a neighbor density.

Given that all of these contracted expressions yield representations that are *atom-centered*, the process can be iterated. For example, one could first compute a low-order  $|\rho_i^{\otimes\nu}\rangle$  descriptor, use it to evaluate the GC representation  $|\rho_i^{\otimes[\nu \leftarrow \nu]}\rangle$ , and then repeat. Depending on how one describes the central atom and the neighbors, the procedure yields  $|\rho_i^{\otimes[\nu \leftarrow [\nu \leftarrow \nu]]}\rangle$ ,  $|\rho_i^{\otimes[[\nu \leftarrow \nu] \leftarrow \nu]}\rangle$  or  $|\rho_i^{\otimes[\nu \leftarrow \nu] \leftarrow [\nu \leftarrow \nu]}\rangle$  (see the SM for a

full expansion of these representations). Each of these descriptors — as well as countless variations in which primitive features of different body order, describing atoms, bonds or general clusters, are combined together — is associated with a tensor product string in the form of Eq. (2). This can be manipulated to improve the efficiency of the calculation, or simply used to characterize the overall body order corresponding to a given architecture.

*c. Scalar terms.* The discussion this far focuses on the case of *equivariant* GC representations that aim to provide a complete basis for symmetric function of the neighbor positions. Arguments similar to those exposed in Eq. (8) make it possible to determine the precise form of the function of interatomic distance vectors that is associated with each type of features. If one relaxes the requirement that the features should provide a well-defined *linear* basis, the architecture can be enriched by including arbitrary non-linear functions, applied to the scalar (invariant) component of the equivariants of any type and order. As a simple example, Behler-Parrinello neural networks<sup>31</sup> compute atom-centered symmetry functions that are equivalent to  $|\rho_i^{\otimes 1}\rangle$  and  $|\rho_i^{\otimes 2}\rangle$ , and use them as inputs to a feed-forward neural network, that is essentially a non-linear function with adjustable parameters. To see what these non-linear terms do, we start from a vector of invariants  $\xi(A) = \{\xi_q(A)\} = \{\langle q|A \rangle\}$  (e.g.  $\{\langle q|\rho_i^{\otimes 2}\rangle\}$  or  $\{\langle q|\rho_i^{\otimes[1 \leftarrow 1]}\rangle\}$ ) and apply Eq. (5), with all terms truncated to  $\lambda = 0$ . This generates all possible products of the initial features  $\langle q_1; q_2 | A^{\otimes 2} \rangle \propto \langle q_1 | A \rangle \langle q_2 | A \rangle$ . In terms of the feature vector, this corresponds to  $\{\xi_1^2, \xi_1 \xi_2, \xi_2^2, \dots\}$ . Repeating the iteration  $k$  times generates all monomials of total order  $k$  that combine powers of  $\{\xi_q\}$ , e.g.  $\xi_1^3 \xi_2^2 \xi_9^{k-5}$ . Comparing with the power series expansion of an analytical function of  $\xi(A)$

$$f(\xi) = \sum_{k_1 k_2 \dots} \frac{f^{(k_1, k_2, \dots)}(0)}{k_1!, k_2!, \dots} \xi_1^{k_1} \xi_2^{k_2} \dots, \quad (12)$$

one sees that computing  $f(\xi)$  is equivalent to repeating the truncated iteration to infinity and projecting the resulting features on the expansion coefficients. Given that  $f$  (and hence the coefficients) usually depends on adjustable parameters, architectures that include scalar functions escape the systematic classification that we propose for equivariant frameworks that are entirely based on the angular momentum iteration. Still, the spirit is clear: each non-linear scalar function brings in infinite body-order correlations, that are however restricted to  $\lambda = 0$  iterations and projected along a single adjustable direction in the infinite-body-order feature space.

## II. EXAMPLES

We choose two simple examples to illustrate the behavior of the GC representations in the context of linear models (details are given in the SM). To test the convergence of the body-order expansion we

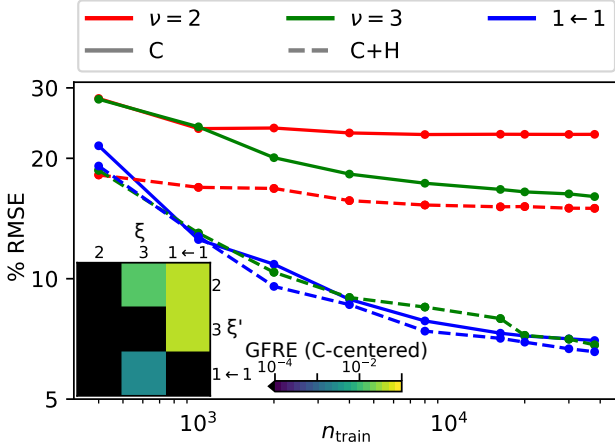


Figure 4: Learning curves for the atomization energy of random  $\text{CH}_4$  configurations, for different C-centered features (full-lines) and for multi-center models using both C and H-centered features (dashed lines). The inset shows the GFRE<sup>32</sup> between different types of C-centered features, i.e. the fractional error made when using features  $\xi(A)$  to linearly predict features  $\xi'(A)$  for the same configurations.

use a dataset of 40,000 random  $\text{CH}_4$  configurations<sup>33</sup>, with energies computed at the DFT level. We discretize the neighbor density on  $n_{\text{max}} = 6$  optimal radial functions<sup>34</sup>, and  $l_{\text{max}} = 4$  angular channels. We set  $r_{\text{cut}} = 3.5 \text{ \AA}$ , so that all atoms are included in each neighborhood.<sup>35</sup> An interesting observation in Ref. 27 is the fact that linear models based on C-centered  $\nu = 4$  features – that should be complete in terms of expanding a symmetric function of the H coordinates – show saturation of the test error at around 4% RMSE. Models based on  $\nu = 3$  features saturate at 8% RMSE. This saturation is related to the truncation of the basis, and is even more evident here (Fig. 4) where we use smaller  $(n_{\text{max}}, l_{\text{max}})$  to enumerate the full 1-center-3-neighbors correlations,<sup>36</sup> and the  $\nu = 3$  model cannot improve beyond 16% RMSE (Fig 4).

GC representations  $[1 \leftarrow 1]$  perform dramatically better, reaching a 7% RMSE. This appears to be due to better convergence of the discretization, and not on modulation of the weight of contributions at different distances, which does change the accuracy of the model (see the SM) but not in terms of the relative performance of  $\nu = 3$  and GC features. This is also evidenced by the global feature space reconstruction error<sup>32</sup> (GFRE) plot: even though  $\nu = 3$  and  $[1 \leftarrow 1]$  ACDC both provide a full basis to expand a three-neighbors symmetric function, with a finite basis set they contain complementary information, and the GC features are substantially more informative than the bispectrum. Using a multi-center model (Fig 4, bottom panel) eliminates almost entirely the advantage of GC features over the bispectrum, consistent with the interpretation that the H-centered density provides a faster-converging description of the interaction between pairs of hydrogen atoms that are far from the

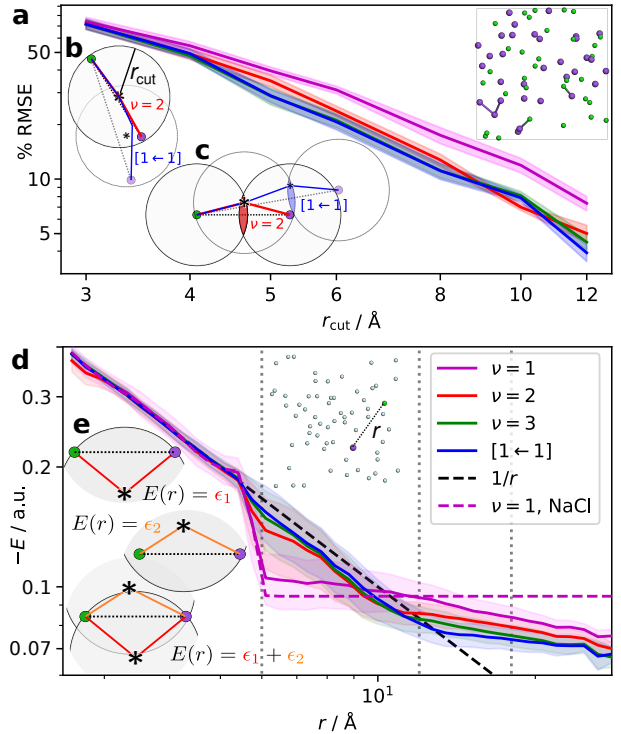


Figure 5: (a) Convergence of the  $n_{\text{train}} = 1800$  validation error for the electrostatic energy of randomized NaCl structures, as a function of  $r_{\text{cut}}$ . The curves correspond to different types of features, following the key in the legend. Shading indicates the standard deviation over three random splits. (b) Schematic of a configuration for which a  $\nu = 2$  (or  $[1 \leftarrow 1]$ ) representation can encode information on a distance  $r > r_{\text{cut}}$ ; (c) to have information on the pair, the central (and the decorated neighbor) atoms must lie in very narrow regions, highlighted. (d) Predicted energy of a single NaCl pair surrounded by inert atoms as a function of the distance, for linear models built on  $r_{\text{cut}} = 6 \text{ \AA}$  features. The line and the shading indicate the conditionally-averaged mean of predictions for a given distance, and a one-standard-deviation range around it. (e) An example of how the same distance can be represented by multiple 3-body terms. Regressing  $E(r)$  in terms of the He-centered contributions,  $\epsilon_1$  and  $\epsilon_2$ , leads to an over-determined system.

C.<sup>27</sup> The GC construction may become advantageous when learning atom-centered properties rather than a decomposition of a global property.

A separate issue is the ability of GC features to incorporate long-range correlations, which we investigate considering a dataset of 2'000 random NaCl bulk configurations<sup>37</sup>, with energies computed as the bare Coulomb interactions between  $\pm e$  charges. This system entails very long-ranged, but perfectly two-body, interactions. Thus,  $|\rho_i^{\otimes 1}\rangle$  invariant features can learn perfectly well the electrostatic energy, although a very large cutoff is necessary to reduce the error below 10% RMSE (Fig. 5a). Frameworks that explicitly incorporate a long-range component<sup>37,38</sup> are

needed to achieve high-accuracy models. It is often stated that  $\nu \geq 2$  features contain information on atoms that are up to  $2r_{\text{cut}}$  apart<sup>39,40</sup>. This is formally true, if the two atoms are simultaneously neighbors of a third (Fig. 5b). Similarly,  $[1 \leftarrow 1]$  GC features can in principle describe correlations up to  $3r_{\text{cut}}$ , and message-passing schemes are often cited as a way to incorporate long-range physics in atomistic ML. However, Fig. 5a clearly shows that increasing the range of interactions indirectly is much less effective than just using a large  $r_{\text{cut}}$  with  $\nu = 1$ .

To better understand this observation, we modify the structures by (1) removing periodic boundary conditions and (2) leaving only one NaCl pair, turning all other atoms to inert “He”, which we assume to not contribute to the target energy but use as environment centers. The energy of each structure is just  $-E(A) = 1/r_{\text{NaCl}}$ . Only a model that uses  $\nu = 1$  features that describe Na and Cl, *ignoring completely the spectator atoms*, yields the expected behavior, fitting the target almost exactly until  $r = r_{\text{cut}}$ , and then becoming constant ( $\nu = 1$ , NaCl in Fig. 5d). Including He atoms within  $\nu = 1$  features gives the predicted  $E(r)$  curve a small slope for  $r > r_{\text{cut}}$ : this is because the atom distribution is not entirely random - there is an “exclusion zone” of 2.5 Å around each atom, and so information on the relative position of He around Na indirectly indicates the possible presence of a Cl atom outside the cutoff. At least with a linear model, using this information leads to a degradation of the quality of the fit at short  $r$ , even though overall the validation-set RMSE decreases. Features with  $\nu \geq 2$  improve the accuracy beyond  $r_{\text{cut}}$ , but there is a large spread around the target, even if all these results are obtained in the large  $n_{\text{train}}$  limit. We believe there are two reasons why the usual argument that 3-body features extend the range of interactions is too simplistic. First, to have some information on  $r_{\text{NaCl}}$  the He atom should be placed in a very precise region, which is increasingly unlikely as  $r$  approaches  $2r_{\text{cut}}$  (Fig. 5c). Second, using a 3-body term to describe the Na–Cl interactions may lead to contradictory scenarios (Fig. 5e). Similar arguments apply to  $[1 \leftarrow 1]$  GC features, that indeed increase only marginally the accuracy of predictions for large  $r$ . This analysis suggests that a fully equivariant GC construction is not necessarily an efficient route to describe long-range/low-body-order interactions, even though it provides, in principle, a systematically convergent basis to express them.

### III. CONCLUSIONS

The formalism we introduce in this work extends the atom-centered density-correlation representations, and their link with linear models of functions of interatomic displacements, to the case in which infor-

mation on multiple environments is combined in a similar symmetry-adapted construction. The scheme captures the key ingredients of equivariant graph-convolution/message-passing ML architectures, which however usually include additional scalar terms that make them more flexible, but prevent establishing a clear correspondence with body-ordered expansions. We illustrate the behavior of the simpler GC representations on two elementary examples – the first focusing on the description of short-range body-ordered interactions, the second on long-range properties. The examples suggest that GC representations can incorporate information on the position of atoms more efficiently than single-atom-centered features, but that this advantage is much reduced when using a multi-center decomposition of a global target property. The analysis of a purely electrostatic learning problem provides insights on the ability of GC features to incorporate long-range correlations. The formal observation that correlations between multiple neighbors extend the range of interactions beyond the cutoff appears to be of limited practical relevance. We expect that this framework will help rationalize and classify geometric message-passing machine-learning schemes, that are often touted as “features-free” approaches, but usually entail the *ad hoc* construction of heavily-engineered architectures. From this point of view, the main challenge is to study systematically the role played by scalar terms – that correspond to infinite correlation order, but restricted to a truncated basis – and the iteration of the MP step, that also requires introducing contractions to limit the size of the feature vectors. A better understanding of the link between different kinds of ML architectures and systematically-converging representations, and between representations and the description of physically-motivated components of the targets, will help in the construction of more accurate, efficient and transferable machine-learning models of atomic-scale problems, as well as all applications that rely on a geometric description of point clouds.

### ACKNOWLEDGMENTS

JN and MC acknowledge support by the NCCR MARVEL, funded by the Swiss National Science Foundation (SNSF) and the European Research Council (ERC) under the European Union’s Horizon 2020 research and innovation programme (grant agreement No 101001890-FIAMMA). GF and JN acknowledge support by the Swiss Platform for Advanced Scientific Computing (PASC). Discussion with Sergey Pozdnyakov and Andrea Grisafi are gratefully acknowledged.

[1] A. V. Shapeev, *Multiscale Model. Simul.* **14**, 1153 (2016).

[2] M. J. Willatt, F. Musil, and M. Ceriotti, *J. Chem. Phys.* **150**, 154110 (2019).

- [3] R. Drautz, Phys. Rev. B **99**, 014104 (2019).
- [4] F. Musil, A. Grisafi, A. P. Bartók, C. Ortner, G. Csányi, and M. Ceriotti, Chem. Rev. **121**, 9759 (2021).
- [5] M. Uhrin, Phys. Rev. B **104**, 144110 (2021).
- [6] M. F. Langer, A. Goeßmann, and M. Rupp, arXiv preprint arXiv:2003.12081 (2020).
- [7] Y. Zuo, C. Chen, X. Li, Z. Deng, Y. Chen, J. Behler, G. Csányi, A. V. Shapeev, A. P. Thompson, M. A. Wood, and S. P. Ong, J. Phys. Chem. A , acs.jpca.9b08723 (2020).
- [8] M. M. Bronstein, J. Bruna, T. Cohen, and P. Veličković, arXiv preprint arXiv:2104.13478 (2021).
- [9] N. Thomas, T. Smidt, S. Kearnes, L. Yang, L. Li, K. Kohlhoff, and P. Riley, arXiv preprint arXiv:1802.08219 (2018).
- [10] F. B. Fuchs, D. E. Worrall, V. Fischer, and M. Welling, arXiv preprint arXiv:2006.10503 (2020).
- [11] J. Gilmer, S. S. Schoenholz, P. F. Riley, O. Vinyals, and G. E. Dahl, in *International Conference on Machine Learning* (2017) pp. 1263–1272.
- [12] K. T. Schütt, F. Arbabzadah, S. Chmiela, K. R. Müller, and A. Tkatchenko, Nature communications **8**, 1 (2017).
- [13] T. Xie and J. C. Grossman, Physical review letters **120**, 145301 (2018).
- [14] N. Lubbers, J. S. Smith, and K. Barros, The Journal of chemical physics **148**, 241715 (2018).
- [15] K. T. Schütt, H. E. Sauceda, P.-J. Kindermans, A. Tkatchenko, and K.-R. Müller, The Journal of Chemical Physics **148**, 241722 (2018).
- [16] O. T. Unke and M. Meuwly, Journal of chemical theory and computation **15**, 3678 (2019).
- [17] L. David, A. Thakkar, R. Mercado, and O. Engkvist, Journal of Cheminformatics **12**, 1 (2020).
- [18] S. Kearnes, K. McCloskey, M. Berndl, V. Pande, and P. Riley, J Comput Aided Mol Des **30**, 595 (2016).
- [19] R. Kondor, H. T. Son, H. Pan, B. Anderson, and S. Trivedi, arXiv preprint arXiv:1801.02144 (2018).
- [20] R. Kondor, Z. Lin, and S. Trivedi, Advances in Neural Information Processing Systems **31**, 10117 (2018).
- [21] B. Anderson, T.-S. Hy, and R. Kondor, arXiv preprint arXiv:1906.04015 (2019).
- [22] S. Batzner, A. Musaelian, L. Sun, M. Geiger, J. P. Mailoa, M. Kornbluth, N. Molinari, T. E. Smidt, and B. Kozinsky, arXiv preprint arXiv:2101.03164 (2021).
- [23] J. Klicpera, J. Groß, and S. Günnemann, arXiv preprint arXiv:2003.03123 (2020).
- [24] Z. Qiao, A. S. Christensen, M. Welborn, F. R. Manby, A. Anandkumar, and T. F. Miller III, arXiv preprint arXiv:2105.14655 (2021).
- [25] J. Nigam, M. J. Willatt, and M. Ceriotti, J. Chem. Phys. **156**, 014115 (2022).
- [26] A derivation for the  $N = 1$  case, that follows closely the ideas in Ref. 1, can be found in Section 4.1 of Ref. 4.
- [27] J. Nigam, S. Pozdnyakov, and M. Ceriotti, J. Chem. Phys. **153**, 121101 (2020).
- [28] K. T. Schütt, M. Gastegger, A. Tkatchenko, and K.-R. Müller, in *Explainable AI: Interpreting, Explaining and Visualizing Deep Learning* (Springer, 2019) pp. 311–330.
- [29] S. N. Pozdnyakov, M. J. Willatt, A. P. Bartók, C. Ortner, G. Csányi, and M. Ceriotti, Phys. Rev. Lett. **125**, 166001 (2020).
- [30] K. Choudhary and B. DeCost, npj Computational Materials **7**, 1 (2021).
- [31] J. Behler and M. Parrinello, Phys. Rev. Lett. **98**, 146401 (2007).
- [32] A. Goscinski, G. Fraux, G. Imbalzano, and M. Ceriotti, Mach. Learn.: Sci. Technol. **2**, 025028 (2021).
- [33] S. Pozdnyakov, M. Willatt, and M. Ceriotti, “Dataset: Randomly-displaced methane configurations,” <https://archive.materialscloud.org/record/2020.110> (2020), (accessed 2020-11-05).
- [34] A. Goscinski, F. Musil, S. Pozdnyakov, J. Nigam, and M. Ceriotti, J. Chem. Phys. **155**, 104106 (2021).
- [35] The H atoms are randomly distributed in a sphere of 3 Å around the central carbon.
- [36] To reduce the complexity of the test, we compute the full invariant correlation features up to  $\nu = 3$ , and the  $|\rho_i^{\otimes[1\leftarrow 1]}\rangle$  GC representations, without any data-driven<sup>27</sup> or heuristic contraction.
- [37] A. Grisafi and M. Ceriotti, J. Chem. Phys. **151**, 204105 (2019).
- [38] A. Grisafi, J. Nigam, and M. Ceriotti, Chem. Sci. **12**, 2078 (2021).
- [39] N. Artrith, T. Morawietz, and J. Behler, Phys. Rev. B **83**, 153101 (2011).
- [40] V. L. Deringer, A. P. Bartók, N. Bernstein, D. M. Wilkins, M. Ceriotti, and G. Csányi, Chem. Rev. **121**, 10073 (2021).